Journal of Materials Chemistry

Cite this: *J. Mater. Chem.*, 2012, **22**, 25154

www.rsc.org/materials

PAPER

The low temperature atomic layer deposition of ruthenium and the effect of oxygen exposure†

Rungthiwa Methaapanon, Scott M. Geyer, Han-Bo-Ram Lee and Stacey F. Bent*

Received 9th August 2012, Accepted 28th September 2012
DOI: 10.1039/c2jm35332f

We have studied the atomic layer deposition (ALD) of ruthenium using bis(2,4-dimethylpentadienyl) ruthenium and oxygen. We show that the process is achievable at a low operating temperature of 185 °C. Variation in the exposure time and pressure of the oxygen counterreactant has significant effects on the nucleation, growth rate and composition of the deposited ruthenium films. High oxygen pressure helps to promote the nucleation of ruthenium on a silicon dioxide substrate. Although saturation conditions are achieved with the Ru precursor, saturation of the ruthenium growth rate with oxygen exposure is observed only for a small range of oxygen exposure. Increasing the oxygen exposure further results in the incorporation of oxygen in the deposited film to form ruthenium oxide, a process which is enhanced at higher deposition temperature. We propose that the slow diffusion of oxygen to the subsurface region is a rate-limiting step in this process. We demonstrate that the composition of the deposited films from metallic ruthenium to ruthenium oxide, as well as the average grain size, may be regulated by tuning the pressure and exposure time of the oxygen counterreactant. Hence, this low temperature ALD process provides a flexible route to the deposition of Ru-based films.

Introduction

Ruthenium is one of the versatile noble metals. It has low bulk resistivity (7 μΩ cm), high work function (4.7 eV)[1–3] and good physical and chemical stability. These properties make ruthenium appropriate for various applications in semiconductor device technologies. Ruthenium has been widely investigated as a potential electrode for dynamic random access memory (DRAM) and ferroelectric random access memory (FRAM), and as a gate electrode material in metal–oxide–semiconductor field effect transistors (MOSFETs).[4] It can also be used as a seed layer for metallization of a copper interconnects.[2] Moreover, the oxide of ruthenium, RuO_2, also finds use in many applications. It has low resistivity (46 μΩ cm) and forms a stable interface with dielectrics, hence is suitable for capacitor electrodes.[5,6] In addition, RuO_2 thin films form an excellent barrier to prevent the diffusion of oxygen.[7]

Most of these applications of Ru and RuO_2 consist of 3D structures at the nano-scale, and they require a deposition technique that can deliver conformal films on a high-aspect ratio framework. Atomic layer deposition (ALD) is one of the thin film deposition techniques most suited for this purpose. It exploits the alternation of self-limiting surface reactions to form a uniform and conformal film that can be well-controlled at the atomic scale.[8,9] Although, in theory, the film by ALD should grow layer by layer and a completely flat film morphology should be achieved, in actual practice, it often grows preferentially on some sites and not others. In addition, the smoothness of the metal film is frequently limited by the formation of coarse crystal grains. Lowering the deposition temperature may help to diminish the distinct crystal growth and provide smoother films.[10] There is evidence that devices with smooth bottom electrodes perform better with lower leakage current.[11] Additionally, low deposition temperatures are required in processes where temperature-sensitive materials are used, such as for interconnect formation on low-*k* dielectrics.[12] Another benefit of low deposition temperature is the smaller contribution from undesirable side reactions like the oxidation of the substrate surface after deposition. Hence it is of interest to develop lower temperature ruthenium ALD process.

It has been reported that a low deposition temperature can be achieved in the platinum ALD process by changing the counterreactant from air to oxygen.[10] However, the use of oxygen has not previously been shown to enhance the growth at low temperature in ruthenium ALD, despite the similarity of the two processes.[4,10] On the other hand, the precursor chemistry plays an important role in determining the process conditions. Many different precursors such as $RuCp_2$,[4,13] $Ru(EtCp)_2$,[5,14] $Ru(thd)_3$,[15] Ru(EtCp)(DMPD),[16–18] and (isopropylmethylbenzene) (cyclohexadiene)Ru have been studied for the deposition of ruthenium

Department of Chemical Engineering, Stanford University, 381 North-South Mall, Stanford, CA 94305, USA. E-mail: bent@stanford.edu; Fax: +1 650 723 9780; Tel: +1 650 723 0385

† Electronic supplementary information (ESI) available: Thickness measurement by SEM and AFM, oxygen pressure and integrated pressure–time of oxygen in the chamber during oxygen the half cycle, the composition of the ruthenium film as sputtered at different time. See DOI: 10.1039/c2jm35332f

by ALD.[2] Most of these precursors required deposition temperatures of at least 250 °C, and the lowest deposition temperature demonstrated in those studies was 220 °C. In this work, we study an ALD process for ruthenium using bis(2,4 dimethylpentadienyl)ruthenium, $Ru(DMPD)_2$, and oxygen. This opened-ring pentadiene precursor has been used for Ru chemical vapor deposition (CVD) processes in the past.[19,20] There has been only one report utilizing this precursor for ALD so far.[21] The deposition in that study was conducted at high operating temperature, which may result in a contribution from a CVD component to the process.

The $Ru(DMPD)_2$ precursor is stable in air and moisture, making its storage and handling simpler than other typical ruthenium precursors. In addition, with this precursor, an unusually low deposition temperature for ruthenium deposition, 185 °C, can be accomplished. Moreover, we can attain either Ru or RuO_2 by changing the deposition conditions. We will discuss the consequence of oxygen exposure, controlled by both time and pressure, on the nucleation and growth of different film compositions.

Results and discussion

The growth characteristics of ruthenium by $Ru(DMPD)_2$ ALD were studied using spectroscopic ellipsometry. In Fig. 1, the thickness of 500 cycle films deposited at 185 °C with 2 s oxygen pulses at 50 mTorr is plotted as a function of $Ru(DMPD)_2$ pulse time. The results show that the thickness saturates by a ruthenium precursor dose of 4 s. This saturation implies a self-limited reaction of $Ru(DMPD)_2$ with the surface, which is one of the important characteristics of an atomic layer deposition process.

Ruthenium film thicknesses grew linearly with the number of ALD cycles but contained a nucleation period as seen in Fig. 2 for two different pressures of the oxygen counterreactant. The data in Fig. 2 are shown for a substrate temperature of 185 °C.

The results of a temperature-dependent study of Ru ALD are shown in Fig. 3. The growth of ruthenium at different temperatures exhibits three regimes. In the lower temperature regime, the growth of ruthenium increases with deposition temperature. No ruthenium growth was observed at temperatures below 165 °C. Between 185 °C and 210 °C, we observed a stable growth regime of ruthenium ALD. Above 210 °C, the growth rate increases once again with temperature. The deposition

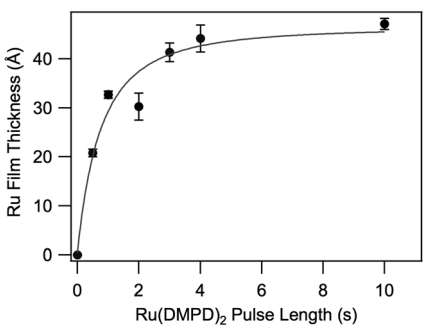

Fig. 1 The thickness of ruthenium films deposited on SiO_2 for various $Ru(DMPD)_2$ pulse lengths. The oxygen pulse was held at 2 s (50 mTorr); surface temperature was 185 °C.

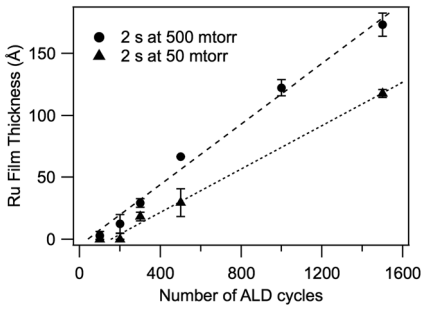

Fig. 2 Growth curves for ALD ruthenium by $Ru(DMPD)_2$ when deposited with 2 s pulses of oxygen counterreactant at 50 mTorr and 500 mTorr pressure, at a surface temperature of 185 °C.

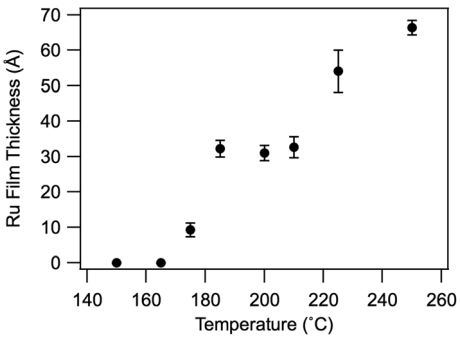

Fig. 3 The temperature dependence of ruthenium growth using $Ru(DMPD)_2$. The thicknesses were measured after 500 ALD cycles.

temperatures at which Ru ALD can be achieved with $Ru(DMPD)_2$ are lower than that of other ALD processes previously reported for ruthenium deposition.[2,22] The low deposition temperature is likely attainable due to the relatively low decomposition temperature of $Ru(DMPD)_2$.[23] The correlation between deposition temperature and precursor decomposition temperature has been previously described by Kawano *et al.* who studied the effect of ruthenium precursor ligands on the MOCVD process and showed that the deposition temperatures tracked the decomposition temperatures of the precursors.[23]

The data in Fig. 2 and 3 indicate that the growth rates of ruthenium using the $Ru(DMPD)_2$ precursor are moderately low. With 500 mTorr of oxygen, we observe a growth rate of 0.12 Å per cycle, while a slightly lower growth rate (0.09 Å per cycle) is observed with 50 mTorr of oxygen. In addition to the lower growth rate, the ruthenium deposition at lower oxygen pressure also shows an increased incubation time (Fig. 2), from ~50 cycles when deposited with 500 mTorr oxygen to ~160 cycles when deposited with 50 mTorr of oxygen.

SEM images of the 500 cycle samples shown in Fig. 4 support a slow nucleation of ruthenium on the SiO_2 surface when 50 mTorr oxygen exposures are used. The overall surface coverage of ruthenium is sparse, and the number of nucleation sites on this sample is clearly lower than those on the sample deposited with 500 mTorr of oxygen. However, the number of ruthenium nucleation sites deposited with both oxygen pressures does not seem to increase noticeably from 500 cycles to 1500 cycles. In addition, after 1500 cycles, a larger grain size in the film deposited at 50 mTorr is clearly observable. These results indicate that

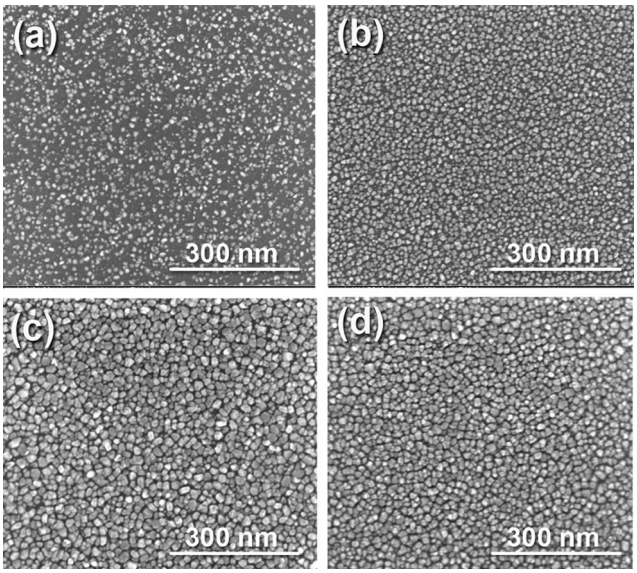

Fig. 4 SEM images of the surfaces after ruthenium deposition at different conditions: (a) 500 ALD cycles ruthenium film deposited at 50 mTorr oxygen; (b) 500 ALD cycles ruthenium film deposited at 500 mTorr oxygen; (c) 1500 ALD cycles ruthenium film deposited at 50 mTorr oxygen and (d) 1500 ALD cycles ruthenium film deposited at 500 mTorr oxygen. All samples were deposited at 185 °C.

ruthenium grows preferentially on previously nucleated sites rather than initiate new nucleation sites, based on the following reasoning. The ruthenium grains will expand until they contact other grains to form a uniform film. When the nuclei on the surface are more distantly spaced, as with 50 mTorr oxygen exposure, the grains will grow larger. This is consistent with the observation of the larger ruthenium grains in the films deposited at a lower pressure of oxygen, since there is a lower density of nucleation sites on the surface.

Despite the different growth rate resulting from changing the oxygen pressure from 50 mTorr to 500 mTorr, the compositions of the deposited films were found to be the same. From Auger electron spectroscopy (AES) depth profiles (Fig. 5), the presence of oxygen in films deposited with 50 mTorr and with 500 mTorr oxygen is only detected at the outer surface of the samples. This oxygen likely originated from surface oxidation of the ruthenium films in air after the deposition, since the majority of the deposited films remains metallic ruthenium. As expected from the different growth rates for the two oxygen conditions, the sputtering time required to remove all the ruthenium from the surface of the sample deposited with 50 mTorr of oxygen is slightly shorter than from the sample deposited with 500 mTorr of oxygen, reflecting a thinner film.

To better understand the behavior of the oxygen counter-reactant, we explored the growth of ruthenium as a function of oxygen pressure and oxygen exposure time. For example, in one study, the pressure of the oxygen counterreactant was raised to 1000 mTorr, while the exposure time was kept at 2 s. In another study, the oxygen pressure was kept at 50 mTorr but with a long exposure time of 30 s. The detailed pressure-*versus*-time curves are shown in ESI.† Because the pressure rise and fall does not occur as a step function during any dose, we must account for the specific exposure profile in these studies. Total exposure is thus

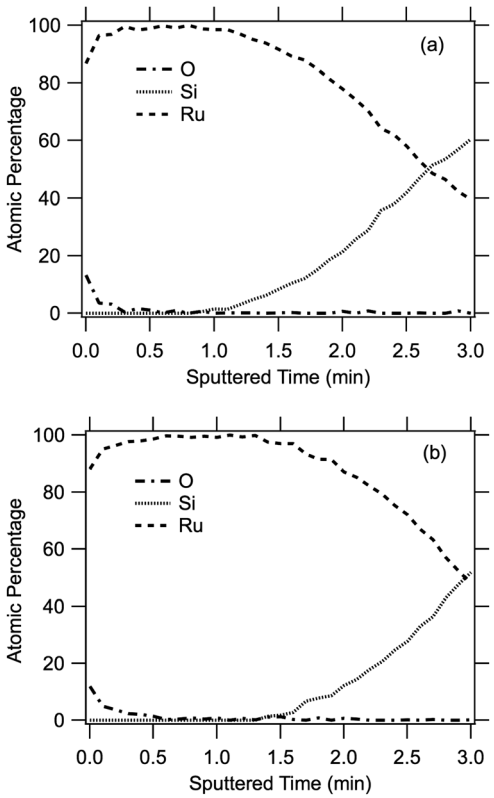

Fig. 5 AES depth profiles of the Ru ALD samples deposited at 185 °C for 1500 cycles with (a) 50 mTorr of oxygen and (b) 500 mTorr of oxygen.

determined by integrating the oxygen pressure over time. The total amount of oxygen as estimated from the integrated pressure–time curve in the chamber is the highest for the case of the 2 s dose at 1000 mTorr, followed by the 30 s dose at 50 mTorr, the 2 s dose at 500 mTorr, the 2 s dose at 300 mTorr, and finally the 2 s dose at 50 mTorr.

The thicknesses *versus* ALD cycle growth curve and growth rate for each set of oxygen exposure conditions are shown in Fig. 6 and 7. Interestingly, the growth rate of ruthenium has a non-monotonic dependence on oxygen exposure. Moreover, the

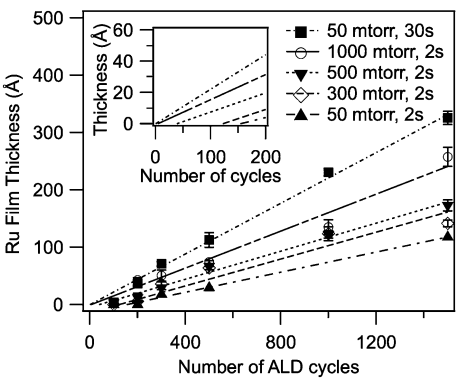

Fig. 6 Growth behavior of ruthenium under various oxygen exposure conditions. The inset displays a magnified plot of the fits to the growth curves at a low number of cycles to show the incubation time under all oxygen conditions.

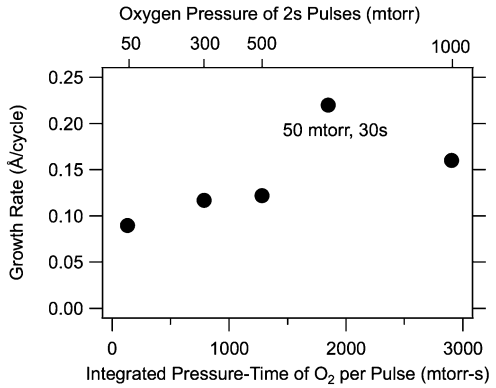

Fig. 7 Growth rate of ruthenium when deposited at 185 °C with 2 s pulses of oxygen at various pressures.

deposited material transitions from metallic ruthenium to ruthenium oxide as a function of oxygen exposure conditions. Ruthenium films grown with 300 mTorr and 500 mTorr of oxygen at 2 s pulses were metallic (*vide infra*), and exhibited similar growth rates of approximately 0.12 Å per cycle. As shown in Fig. 7, the growth rates of the films deposited with 300 mTorr and 500 mTorr increased from that observed with 50 mTorr of oxygen and began to plateau, suggesting that saturation of oxygen was attained under these oxygen conditions. Hence, this regime appears to operate in a classic, self-limiting ALD process. However, once the oxygen pressure was sufficiently high, we observed a noticeable increase in the growth rate of the deposited film again to 0.16 Å per cycle, at 1000 mTorr oxygen. However, the increased growth rate was not proportional to the total oxygen exposure, but rather was more sensitive to pulse time. The growth rate of ruthenium is unexpectedly even higher (0.23 Å per cycle) when 30 s of 50 mTorr of oxygen was used, despite the smaller total oxygen exposure compared to the 1000 mTorr case. The higher growth rate at each of these higher oxygen exposures was accompanied by a transition from deposition of ruthenium metal to deposition of ruthenium oxide (*vide infra*). The films deposited with very long oxygen exposure (30 s) contain primarily RuO_2. Although previous ALD studies using different precursors have shown that high oxygen partial pressure converts the film composition from Ru to RuO_2,[5,24–26] interestingly, those studies did not observe a dependence of oxide formation on oxygen exposure time as we observed here using $Ru(DMPD)_2$. In addition, different results were reported between the various studies: Park *et al.* reported no formation of crystalline RuO_2 phase using $Ru(Cp)_2$,[24] while Kwon *et al.* and Kim *et al.* detected strong RuO_2 features in XRD using $Ru(EtCp)_2$ with high oxygen partial pressures.[5,25] These results suggest that ruthenium oxide formation is strongly influenced by the type of ruthenium precursor.

According to Fig. 6, the nucleation delay also changed with different oxygen exposure conditions. The film deposited with 300 mTorr of oxygen exhibits ~120 cycles delay in the nucleation. This value is between what we observed for the growth with 50 mTorr (~150 cycles) and with 500 mTorr of oxygen (~50 cycles). It is evident that the oxygen pressure has an influence on the nucleation of the ruthenium film. The high oxygen pressure appears to enhance the nucleation of the ruthenium film, likely by increasing the number of nucleation sites, *i.e.* the number of adsorbed oxygen atoms on the surface.

Fig. 8 shows the elemental analysis by XPS of thick films deposited under different conditions. For films grown with 2 s of 500 mTorr of oxygen (Fig. 8a), there are two main peaks detected: the peak at 279.6 eV and the one at 283.7 eV, which belong to the doublet peaks of Ru $3d_{5/2}$ and Ru $3d_{3/2}$ of metallic ruthenium (Ru^0), respectively. The spectrum was dominated by metallic ruthenium under these conditions. A small quantity of oxygen seen in the O 1s spectrum, corresponding to the small Ru 3d peaks at higher binding energy in the Ru 3d spectrum, was also detected. This contribution is likely due to the outer surface oxidation from the air. At higher oxygen exposures (Fig. 8b and c), we observe a broadening of the Ru 3d peaks to higher binding energy, indicating the formation of ruthenium oxide. In this high binding energy regime, two peaks and their associated doublet

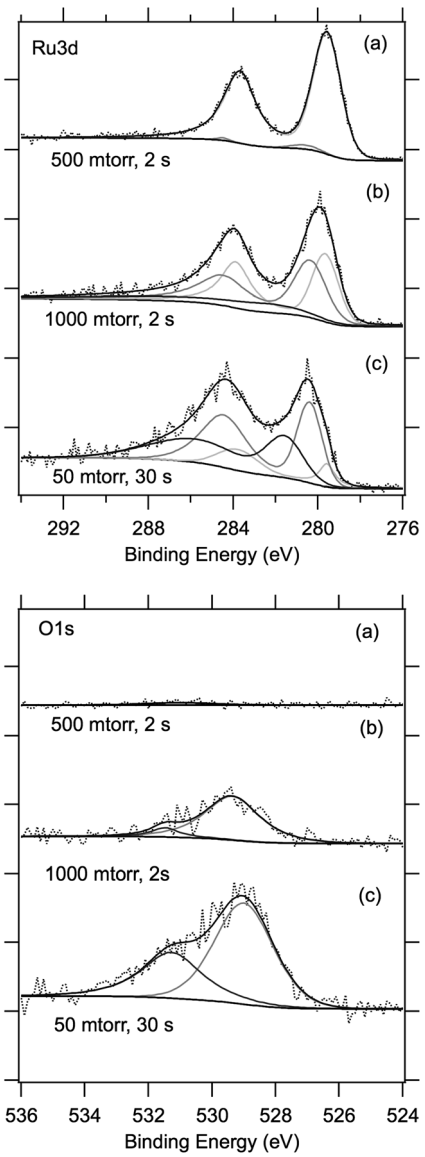

Fig. 8 XPS spectra of the ruthenium film deposited at various oxygen exposure conditions. Spectra were normalized based on the Ru $3d_{5/2}$ peak.

peaks can be assigned. The lower of the two higher binding energy Ru 3d peaks at ~280.4 eV and its doublet at ~284.4 eV are assigned to the Ru^{4+} state of RuO_2.[27] The assignment of the highest binding energy Ru 3d peaks is somewhat complicated. There have been disagreements in the assignment of this peak in the literature. While Kim and Winograd suggested the existence of a higher oxidation state such as RuO_3 and RuO_4,[28] Cox *et al.* proposed that the peak arose from the final-state screening effect of the Ru^{4+} state.[29] The study by Shen *et al.* agreed with the Ru^{4+} double peaks supposition by Cox and also questioned the existence of a RuO_3 state in the film,[30] which is known to be unstable at room temperature. Additionally, Shen *et al.* argued that the higher binding energy O 1s peak should be assigned to dissolved atomic oxygen instead of oxygen bound to a higher oxidation state ruthenium atom. As suggested by Shen *et al.*, the presence of the high binding energy peaks of Ru 3d and O 1s therefore would not be correlated.

In our study, we observed a significant decrease in the intensities of both high binding energy Ru 3d peaks and the high binding energy O 1s peak after sputtering (see ESI†), while the Ru 3d and O 1s peaks associated with RuO_2 (280.4 eV and 529.5 eV, respectively) were barely changed. This evidence suggests the assignment of these peaks to a higher oxidation state ruthenium oxide in the film, similar to the assignment put forth by Kim and Winograd, implying that RuO_3 is a stable surface species on RuO_2.[28] This phase is probably less stable and may have vaporized during the sputtering process leading to the disappearance of the high binding energy peak as the film was sputtered down. Park *et al.* also detected the formation of multivalent ruthenium oxide at higher oxidation state by FTIR spectroscopy, consistent with our study.[31]

We also studied the crystal structure of the deposited films using synchrotron radiation high-resolution XRD with a 12.7 keV beam energy. The results are shown in Fig. 9. Since the energy of the X-ray beam used in these experiments is different from the 8 keV of a typical XRD system using a Cu Kα source, the diffraction peak pattern of a specific crystal structure appears at different 2θ angles. Fig. 9 also shows the diffraction pattern in association with the Q-space in the top axis, as these values are the intrinsic properties that remain the same regardless of the X-ray beam energy. The relationship between Q-space and diffraction angle can be calculated *via* the equation $Q = 4\pi\sin(\theta)/\lambda$.

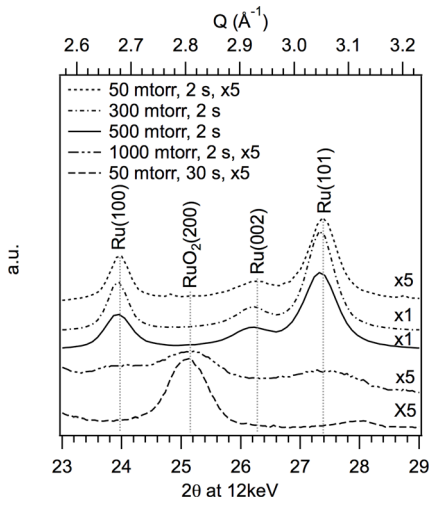

Fig. 9 High resolution X-ray diffraction patterns of ruthenium films deposited under various oxygen exposure conditions at 185 °C.

The XRD results agree well with the elemental analysis by XPS. In the films deposited with 50 mTorr, 300 mTorr and 500 mTorr of oxygen at a 2 s pulse length, we observe peaks at 24.0°, 26.3° and 27.4°, which are assigned to the diffraction of the (100), (202) and (101) planes of the hcp structure of metallic ruthenium. The positions of the peaks are very close to the values predicted by calculation using the lattice constant of bulk ruthenium.[32] The diffraction peak intensities of the film deposited with 50 mTorr oxygen are significantly weaker than those of the film deposited with 300 mTorr and 500 mTorr oxygen, due to the observable difference in the film thicknesses. Interestingly, the diffraction peaks of the films deposited with 300 mTorr oxygen are slightly stronger than those of the film deposited at 500 mTorr oxygen, despite the similar thickness. The average grain size in the ruthenium film grown with 300 mTorr of oxygen, as deduced from the width of the diffraction peaks using a Scherrer analysis, is roughly 90 Å, which is approximately 10 Å larger than those grown with 500 mTorr of oxygen. The smaller grain size at the higher oxygen pressure supports a mechanism of more concentrated nucleation sites during the early stage of the ruthenium growth with the higher-pressure oxygen.

With even higher oxygen exposures, the RuO_2 phase was observed. With 1000 mTorr of oxygen, the crystalline phase of metallic ruthenium was significantly decreased while the rutile phase of RuO_2 grew in. For the longest oxygen exposure time (30 s), we no longer detected the phase related to metallic ruthenium in the film. The diffraction spectra show a strong RuO_2 rutile structure.

The ruthenium oxide detected in the films is in agreement with the growth rates observed. The increased growth rates seen with higher oxygen exposure are likely due to the presence of oxygen in the film. Based on the lattice parameters, changing from the hexagonal closed pack structure of metallic ruthenium to the rutile structure of RuO_2 will lead to a decrease in the atomic density of ruthenium atoms per volume by approximately four times. However, the growth rate also depends on other factors including steric hindrance[33] and crystal structure[34] that can decrease the growth rate from the expected value. We observe an increase in the film growth rate from metallic ruthenium to RuO_2 only by a factor of two, suggesting a smaller number of deposited ruthenium atoms overall.

Nonetheless, the observation of higher growth rate and oxide content in films deposited with long oxygen exposure at low pressure compared to those deposited with short oxygen exposure at high pressure is surprising. Although we do not fully understand the mechanism behind this occurrence, we propose the following possible explanation. The necessity of long oxygen exposure, on the order of seconds, suggests the presence of a very slow step in the deposition process. While oxygen adatoms at the surface likely play a key role in reactions with the incoming ruthenium precursors, the ruthenium oxide phase may be produced *via* subsurface oxygen, as suggested by theoretical studies.[35,36] A subsurface oxygen formation process in ruthenium has been reported in the literature to take place at temperatures

as low as 400 K.[37] The process requires the formation of a complete oxygen adlayer on the top surface prior to the diffusion of oxygen atoms into the subsurface layer, according to a literature report.[38] Since subsurface oxygen formation is associated with multiple steps, including a physical diffusion process, it may involve a longer time scale. The low diffusion rate of oxygen in bulk ruthenium below 1150 K (ref. 39) also supports the requirement of longer oxygen exposure time. Interestingly, despite the long oxygen exposure times required, a fairly low oxygen pressure of 50 mTorr seems to be sufficient to carry out the process. The requirement of a slow mechanistic step in the formation of subsurface oxygen may explain why we do not observe as large RuO_2 content in the film deposited at 1000 mTorr with 2 s exposure as in the film deposited at 50 mTorr with 30 s exposure.

To test this model, we carried out studies to investigate the temperature dependence of the ALD process leading to RuO_2 formation. If ruthenium oxide is formed by subsurface oxygen generated by an activated diffusion process, ALD at higher temperatures should require shorter O_2 exposures to form the oxide. Experiments were performed at 200 °C as a function of oxygen exposure, ranging from 300 mTorr to 1000 mTorr. The results of oxygen to ruthenium ratios in the films deposited at 200 °C are shown in Fig. 10, in comparison to the films deposited at 185 °C and 175 °C. To avoid the complication of surface oxidation under ambient condition, the top surfaces were briefly sputtered prior to analysis. The data show that at higher temperature, lower pressure and shorter time are required for ruthenium oxide formation. A noticeable amount of oxide forms with 2 s of 500 mTorr oxygen at 200 °C, while only a small amount of oxide forms with 2 s of 700 mTorr oxygen at 185 °C. At a lower temperature of 175 °C, no oxide formation is observed even with 2 s of 1000 mTorr oxygen, indicating a strong temperature dependence to the oxide formation. Moreover, at a lower oxygen pressure of 70 mTorr, as shown on the right side of Fig. 10, we observed only partial oxidation of the film at 185 °C with a 15 s oxygen pulse, whereas the O/Ru ratio is slightly above 2, indicating complete oxide formation, with the same oxygen pulse length at 200 °C. These results are consistent with the kinetically rate limiting step that we propose, although it does not rule out a different activated step. If the deposition temperature is sufficiently high, the oxygen exposure time will no longer be the limiting parameter under typical ALD pulse conditions, given the much stronger (exponential) dependence of the process on temperature. This may explain the insignificance of the oxygen exposure time on the oxide formation in other reported studies that were performed at higher temperatures, close to 300 °C.[25,26]

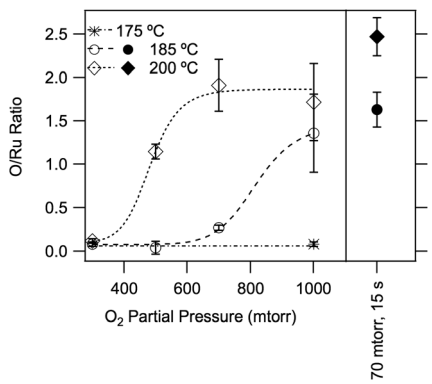

Fig. 10 Ratio of oxygen to ruthenium in the deposited films at different oxygen conditions and temperatures from AES. The dashed curves are guides to the eye. Unless otherwise specified, the duration of the oxygen pulses was 2 s.

Interestingly, extending the ruthenium precursor exposure time in these studies from 4 s to 10 s does not significantly change the composition of the film deposited with 2 s of 1000 mTorr oxygen at 200 °C (as detected by AES, data is not shown), in contrast to the observation by Kwon *et al.* using $Ru(EtCp)_2$ and oxygen in which the deposited films turned into metallic ruthenium upon extended ruthenium precursor exposure.[25,26]

Experimental section

The Ru/RuO_2 films were deposited on n-type Si (100) wafers (ρ = 1.0–5.0 Ω cm), which were sequentially rinsed in acetone ($OC(CH_3)_2$) and ethanol (C_2H_5OH), followed by piranha cleaning (30 : 70, 30% H_2O_2 : H_2SO_4). This process resulted in a chemical oxide of silicon on the top surface of the substrates that was free from carbon contamination. All reactions were carried out in a custom built, warm-wall ALD reactor, at deposition temperatures ranging from 165 °C to 250 °C. Bis(2,4-dimethylpentadienyl)ruthenium(II) (99%, Sigma-Aldrich) was kept in a delivery vial at 60 °C, while the manifold line was maintained at 70 °C to minimize condensation in the line. Oxygen (99.999%, Praxair) was used as a counterreactant, while nitrogen was used as carrier and purging gas.

The thicknesses of the deposited films were estimated from spectroscopic ellipsometry (Woolam α-SE) by using a Drude–Lorentz model with three harmonic oscillators which is suitable for conductive films.[40,41] A layer of surface roughness consisting of 50% voids was assumed on the top surface. The calculated thicknesses were compared to the thicknesses of selected films observed by cross-sectional scanning electron microscope (SEM) and by atomic force microscopy (AFM), by scraping off the film and measuring the height difference between the area with and without the deposited films. The differences between the thickness estimated by spectroscopic ellipsometry and the other two techniques were found to agree within 20%. The morphology of the ruthenium films was investigated visually by SEM (FEI Magellan 400 XHR Scanning Electron Microscope), while X-ray diffraction (XRD) was used to determine the crystallographic structure of the films. The XRD was conducted with high resolution using synchrotron radiation at the Stanford Synchrotron Radiation Lightsource (SSRL), beamline 7-2, with photon energy of 12.7 keV. All films analyzed by XRD were deposited with 1000 ALD cycles at specified conditions, which resulted in films of thicker than 10 nm.

Elemental analyses were performed by X-ray photoelectron spectroscopy (SSI S-probe XPS spectrometer) for the overall film analysis and by Auger electron spectroscopy (PHI 700 Scanning Auger Nanoprobe) for depth profiling. AES was also used to obtain the oxygen-to-ruthenium ratios in the temperature dependent studies; these ratios were calibrated by a RuO_2 sample as confirmed by XRD. Note that the prominent photoemission peak of ruthenium is in close proximity to the peak of carbon,

both in XPS (Ru 3d and C 1s) and in AES (Ru MVV and C KVV). This peak coincidence complicated the data analysis, especially when both ruthenium and carbon were expected. High-resolution scans together with detailed peak fittings were used for XPS data analysis to resolve ruthenium peaks from carbon peak. For AES, the spectra were collected in differential form, making the peak fitting process impractical. The ruthenium spectra were collected both at 276 eV (MVV) and at 231 eV (MNV), where it was not under the influence of the photoemission peak of other elements. The depth profiles calculated from the two regions were compared to determine the presence of carbon.

Conclusions

Films of metallic ruthenium and ruthenium oxide were grown by ALD at low deposition temperature using $Ru(DMPD)_2$ and oxygen. The process was highly dependent on the oxygen exposure. Oxygen reacted with $Ru(DMPD)_2$ to form metallic ruthenium when short oxygen pulses and low oxygen pressures were utilized. With higher oxygen pressures and longer exposure time, the process was found to deposit ruthenium oxide. Prolonged oxygen exposure is found to be more effective than short intense exposure in producing ruthenium oxide, and we propose that the slow diffusion of oxygen into the film to form sub-surface oxygen is a rate-limiting step in the oxide formation. Studies at elevated temperature support the presence of an activated step involving oxygen in the formation of the ruthenium oxide. During the nucleation step, a high oxygen pressure was required to produce sufficient nucleation sites for the ruthenium precursor to react at, and the nucleation density of Ru deposited at lower oxygen pressures was sparser than that deposited at higher oxygen pressures. The nucleation step is also important in determining the grain size of the crystalline ruthenium film since ruthenium grew preferentially on previously nucleated sites. Overall, we have demonstrated a new ALD process for deposition of Ru and RuO_2 applicable at relatively low temperatures, in which the composition and the morphology of the film can be controlled by adjusting the oxygen exposure conditions.

Acknowledgements

The work was supported by the Department of Energy under Award Number DE-SC0004782. RM gratefully acknowledges the Anandamahidol Foundation Graduate Fellowship. Portions of this research were carried out at the Stanford Synchrotron Radiation Lightsource, a Directorate of SLAC National Accelerator Laboratory and an Office of Science User Facility operated for the U.S. Department of Energy Office of Science by Stanford University. The authors gratefully express appreciation to Steve Herron and Nuoya Yang for their assistance on AES experiments.

Notes and references

1 K. Gregorczyk, L. Henn-Lecordier, J. Gatineau, C. Dussarrat and G. Rubloff, *Chem. Mater.*, 2011, **23**, 2650–2656.
2 T.-K. Eom, W. Sari, C. Kyu-Jeong, S. Woong-Chul, K. Jae Hyun, L. Do-Joong, K. Ki-Bum, S. Hyunchul and K. Soo-Hyun, *Electrochem. Solid-State Lett.*, 2009, **12**, 85–88.
3 J. Kim and T. W. Kim, *JOM*, 2009, **61**, 17–22.
4 T. Aaltonen, P. Alen, M. Ritala and M. Leskela, *Chem. Vap. Deposition*, 2003, **9**, 45–49.
5 W. H. Kim, S. J. Park, D. Y. Kim and H. Kim, *J. Korean Phys. Soc.*, 2009, **55**, 32–37.
6 P. Lu, S. He, F. X. Li and Q. X. Jia, *Thin Solid Films*, 1999, **340**, 140–144.
7 L. Krusin-Elbaum, M. Wittmer and D. S. Yee, *Appl. Phys. Lett.*, 1987, **50**, 1879–1881.
8 S. M. George, *Chem. Rev.*, 2009, **110**, 111–131.
9 M. Leskela and M. Ritala, *Thin Solid Films*, 2002, **409**, 138–146.
10 T. Aaltonen, M. Ritala, Y.-L. Tung, Y. Chi, K. Arstila, K. Meinander and M. Leskelä, *J. Mater. Res.*, 2004, **19**, 3353–3358.
11 C. S. Hwang, *Mater. Sci. Eng. B*, 1998, **56**, 178–190.
12 K. E. Elers, V. Saanila, P. J. Soininen, W. M. Li, J. T. Kostamo, S. Haukka, J. Juhanoja and W. F. A. Besling, *Chem. Vap. Deposition*, 2002, **8**, 149–153.
13 K. J. Park, D. B. Terry, S. M. Stewart and G. N. Parsons, *Langmuir*, 2007, **23**, 6106–6112.
14 S. S. Yim, D. J. Lee, K. S. Kim, S. H. Kim, T. S. Yoon and K. B. Kim, *J. Appl. Phys.*, 2008, **103**, 113509.
15 T. Aaltonen, M. Ritala, K. Arstila, J. Keinonen and M. Leskelä, *Chem. Vap. Deposition*, 2004, **10**, 215–219.
16 S. K. Kim, S. Y. Lee, S. W. Lee, G. W. Hwang, C. S. Hwang, J. W. Lee and J. Jeong, *J. Electrochem. Soc.*, 2007, **154**, D95–D101.
17 J. Heo, S. J. Won, D. Eom, S. Y. Lee, Y. B. Ahn, C. S. Hwang and H. J. Kim, *Electrochem. Solid-State Lett.*, 2008, **11**, H210–H213.
18 S. K. Kim, J. H. Han, G. H. Kim and C. S. Hwang, *Chem. Mater.*, 2010, **22**, 2850–2856.
19 K. Kawano, H. Kosuge, N. Oshima and H. Funakubo, *Electrochem. Solid-State Lett.*, 2007, **10**, D60–D62.
20 L. Meda, R. C. Breitkopf, T. E. Haas and R. U. Kirss, *Mater. Res. Soc. Symp. Proc.*, 1997, **495**, 75–80.
21 O. van der Straten, S. M. Rossnagel, J. P. Doyle and K. P. Rodbell, *ECS Trans.*, 2006, **1**, 51–56.
22 S. K. Kim, S. Han, G. H. Kim, J. H. Jang, J. H. Han and C. S. Hwang, *J. Electrochem. Soc.*, 2011, **158**, D477–D481.
23 K. Kawano, H. Kosuge, N. Oshima and H. Funakubo, *Electrochem. Solid-State Lett.*, 2009, **12**, D80–D83.
24 S.-J. Park, W.-H. Kim, W. J. Maeng, Y. S. Yang, C. G. Park, H. Kim, K.-N. Lee, S.-W. Jung and W. K. Seong, *Thin Solid Films*, 2008, **516**, 7345–7349.
25 O. K. Kwon, J. H. Kim, H. S. Park and S. W. Kang, *J. Electrochem. Soc.*, 2004, **151**, G109–G112.
26 S. H. Kwon, O. K. Kwon, J. H. Kim, S. J. Jeong, S. W. Kim and S. W. Kang, *J. Electrochem. Soc.*, 2007, **154**, H773–H777.
27 *NIST X-ray Photoelectron Spectroscopy Database, Version 3.5*, National Institute of Standards and Technology, Gaithersburg, 2003, http://srdata.nist.gov/xps/.
28 K. S. Kim and N. Winograd, *J. Catal.*, 1974, **35**, 66–72.
29 P. A. Cox, J. B. Goodenough, P. J. Tavener, D. Telles and R. G. Egdell, *J. Solid State Chem.*, 1986, **62**, 360–370.
30 J. Y. Shen, A. Adnot and S. Kaliaguine, *Appl. Surf. Sci.*, 1991, **51**, 47–60.
31 S. K. Park, R. Kanjolia, J. Anthis, R. Odedra, N. Boag, L. Wielunski and Y. J. Chabal, *Chem. Mater.*, 2010, **22**, 4867–4878.
32 S. Brennan and P. L. Cowan, *Rev. Sci. Instrum.*, 1992, **63**, 850–853.
33 M. Leskela and M. Ritala, *Angew. Chem., Int. Ed.*, 2003, **42**, 5548–5554.
34 A. Crown, C. Johnston and A. Wieckowski, *Surf. Sci.*, 2002, **506**, L268–L274.
35 K. Reuter, C. Stampfl, M. Veróonica Ganduglia-Pirovano and M. Scheffler, *Chem. Phys. Lett.*, 2002, **352**, 311–317.
36 M. Todorova, W. X. Li, M. V. Ganduglia-Pirovano, C. Stampfl, K. Reuter and M. Scheffler, *Phys. Rev. Lett.*, 2002, **89**, 096103.
37 G. Praline, B. E. Koel, H. I. Lee and J. M. White, *Appl. Surf. Sci.*, 1980, **5**, 296–312.
38 A. Bottcher and H. Niehus, *J. Chem. Phys.*, 1999, **110**, 3186–3195.
39 I. J. Malik and J. Hrbek, *J. Phys. Chem.*, 1991, **95**, 10188–10190.
40 P. Hones, T. Gerfin and M. Gratzel, *Appl. Phys. Lett.*, 1995, **67**, 3078–3080.
41 M. Knaut, M. Junige, M. Albert and J. W. Bartha, *J. Vac. Sci. Technol., A*, 2012, **30**, 01A151–01A159.

